Numerical Modeling of Electrodeless Electric Thruster by Ion Cyclotron Resonance/Ponderomotive Acceleration*)

Fumiko OTSUKA, Tohru HADA, Shunjiro SHINOHARA[1], Takao TANIKAWA[2] and
Takeshi MATSUOKA[3, a]

Interdisciplinary Graduate School of Engineering Sciences, Kyushu University, Kasuga, Fukuoka 816-8580, Japan
[1]*Institute of Engineering, Tokyo University of Agriculture and Technology, Koganei, Tokyo 184-8588, Japan*
[2]*Research Institute of Science and Technology, Tokai University, Hiratsuka, Kanagawa 259-1292, Japan*
[3]*Japan Aerospace Exploration Agency, Sagamihara, Kanagawa 252-5210, Japan*

We developed an electrodeless electric thruster that utilizes ion cyclotron resonance/ponderomotive acceleration (ICR/PA) for ion acceleration. We conducted test particle simulations to assess the thruster's performance. We compared the thrusts obtained using argon (Ar) and helium (He) gas as propellants at the same mass flow rate. On the basis of a model that includes ion wall loss and ion-neutral collisions, we estimated the exhaust velocity and thrust. We found that He ions are less influenced by both ion wall loss and ion-neutral collisions than are Ar ions because the gyroradii of He ions are generally smaller than those of Ar ions and the ratio of the gyrofrequency to the collision frequency for He ions is larger than that for Ar ions. In addition, the exhaust velocities of He ions are larger than those of Ar ions, as predicted by the quasilinear theory and ponderomotive potential. Consequently, the thrust and specific impulse for He are larger than those for Ar.

1. Introduction

The erosion of electrodes in electric thrusters is a serious problem because such erosion limits the lifespan of the thruster. To overcome this problem, "electrodeless" electric thrusters have been extensively studied worldwide in various projects [1–3]. In an electrodeless electric thruster, plasmas are accelerated by external electromagnetic fields, and they are not in contact with the electrodes, which are placed outside the plasma region (see Fig. 1). Thus, the erosion of the electrodes is avoided. As part of the Helicon Electrodeless Advanced Thruster (HEAT) project, we have examined one type of electrodeless plasma acceleration schemes, namely the ion cyclotron resonance/ponderomotive acceleration (ICR/PA), by utilizing test particle simulations [4]. The PA gives rise to a pure parallel acceleration of ions [5], whereas the ICR causes perpendicular ion heating, followed by an energy conversion from the perpendicular to parallel direction in the presence of a divergent magnetic field.

While a well-known application of the ICR to electric thrusters is the Variable Specific Impulse Magnetoplasma Rocket (VASIMR) [2], we have focused on the ponderomotive effect on ion acceleration, although the PA and ICR are inseparable. From the test particle simulations for argon (Ar) ions [4], we have found that the PA can raise the energy gain in the ICR/PA scheme by up to 60% compared with the ICR-only case, when the externally applied rf electric field intensity, E_0, is increased to 1000 V/m. However, the ion gyroradius also increases with the increase in E_0 because of ICR heating; as a result, most ions are lost at the radial wall of the chamber. Consequently, the ions accelerated by the ICR/PA cannot be exhausted from the acceleration region of the chamber. On the other hand, the VASIMR experiments have successfully demonstrated the large acceleration of ions within the parameters necessary to minimize ion wall loss. Namely, in the VASIMR experiments [2], the ion gyroradius is reduced in the following two ways: 1) choosing a light propellant species such as helium (He) or deuterium, and 2) using an intense background magnetic field on the order of 0.25 T, so that the ion wall loss effect can be minimized. However, the latter method leads to an increased weight of the propulsion system, which is a disadvantage in the development of a lightweight thruster. In this paper, we consider the first method to reduce the ion wall loss effect, and discuss the dependence of an ICR/PA thruster's performance on propellant species by using He and Ar as propellants. The thrusts for the two propellants are estimated, along with the effects of ion wall loss and ion-neutral collisions.

---

author's e-mail: otsuka@esst.kyushu-u.ac.jp
[a] present address: Photon Pioneers Center in Osaka University, Suita, Osaka 565-0871, Japan
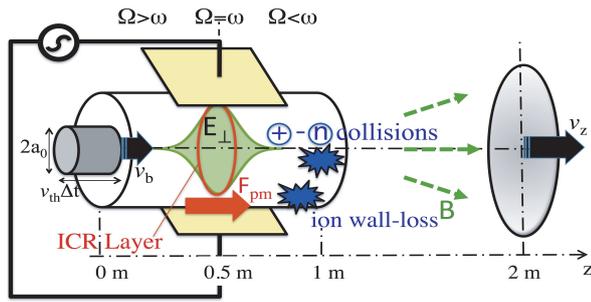*) This article is based on the presentation at the 22nd International Toki Conference (ITC22).

Fig. 1 Schematic picture of the ion cyclotron resonance/ponderomotive acceleration (ICR/PA) scheme.

2. Numerical Model

In this study, we performed the test particle simulations of ions in an external electromagnetic field. Although the numerical model is similar to that of a previous paper [4], there are some differences between the present model and the previous one, which are as follows. First, two ion species are considered: singly ionized ions of both He and Ar. Second, the initial velocities of the test particles are given by a Maxwellian distribution with no drift (or shift) in order to obtain the same mass flow rates of He and Ar ions, whereas those in the previous model were given by a Maxwellian distribution shifted along the axial direction. In this section, we briefly explain the present model.

A schematic picture of our model is depicted in Fig. 1. The ions produced by a helicon wave (not shown in the figure) are injected into an acceleration region through the cylindrical chamber from the left-hand side at $z = 0$ m. Neutral particles fill the chamber uniformly. Electrodes (shown in yellow in the figure) are placed outside the plasma acceleration region, so that the erosion of the electrodes can be avoided. A background magnetic field is oriented mainly along the z-axis, and a linearly polarized transverse rf electric field is applied with its magnitude $E_\perp(z)$ given by a Gaussian shape. The injected ions can be heated perpendicularly, because they travel through the ion cyclotron resonance region; subsequently, their perpendicular energy can be converted into parallel energy in the divergent magnetic field, producing the thrust. In addition, the ions are accelerated along the z-axis by the ponderomotive potential, $\Phi = q_i^2 E_\perp(z)^2/4m_i(\omega^2 - \Omega_i(z)^2)$, where ω is the frequency of the externally applied rf field, and m_i, q_i, and Ω_i are the mass, charge, and the gyrofrequency of the ions, respectively. Here Ω_i decreases along the z-axis, and the resonance point, z_0, at which $\omega = \Omega_i(z_0)$, coincides with the peak of $E_\perp(z)$. The sign of Φ is reversed at the peak; consequently, the ponderomotive force, $F_{pm} = -d\Phi/dz$, becomes unidirectional, leading to a parallel energy gain of the ions [5].

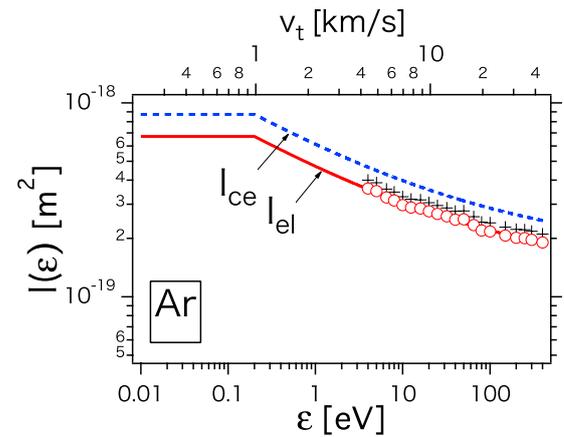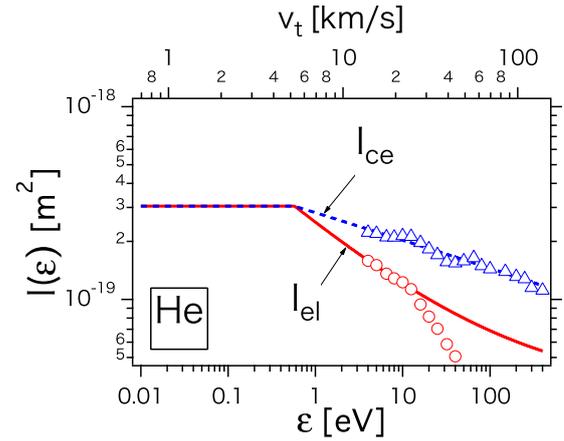The important field parameters are background magnetic field intensity at the resonance, B_0, axial divergent

Fig. 2 Cross-section of charge exchange and elastic collisions for (top) He-He$^+$ and (bottom) Ar-Ar$^+$.

scale length of the background magnetic field, L_B, maximum intensity of the electric field, E_0, and width along the z axis of the electric field, L_E. We fix the parameters $B_0 = 400$ G, $L_B = 1$ m, and $L_E = 0.1$ m, and then evaluate the thrust by varying E_0. The radius and length of the chamber are assumed to be 0.1 m and 1 m, respectively. For both He and Ar ions, we integrate the equation of motion for the ions under the external electromagnetic field described above. The gyrofrequencies of the ions are $\Omega_{He} \sim 10^6$/s and $\Omega_{Ar} \sim 10^5$/s for the He and Ar ions, respectively. The simulation used a time step of $\Delta t_i = 0.01/\Omega_i$ by using the Ω_i for each species.

In our test particle simulations, we include the effects of ion wall loss and ion-neutral collisions. For ion wall loss, the absorbing boundary condition is used. For ion-neutral collisions, the Monte Carlo collision model described by Vahedi and Surendra [6] is used. In this collision model, the collision probability is given as $p = \exp(-\nu_i \Delta t_i)$, where $\nu_i = n_n I(\varepsilon_i) v_{t,i}$ is the collision frequency, n_n is the number density of neutral particles, $I(\varepsilon_i)$ is the collision cross-section as a function of the ion kinetic energy, $\varepsilon_i = m_i v_{t,i}^2/2$, and $v_{t,i}$ is the speed of the ion. We consider two types of collisions: elastic collisions

and charge exchange. Figure 2 shows the collision cross-sections, $I(\varepsilon)$, for (top) He and (bottom) Ar. The solid red and dashed blue lines in each panel show $I(\varepsilon)$ for the elastic collisions and charge exchange, respectively. These cross-sections are used in our calculations, and are obtained by fitting the experimental data [7, 8] which are indicated in the figures by the empty circles and triangles. The "+" symbols in the bottom panel show the experimental data used in our previous paper [4].

The slight difference in $I(\varepsilon)$ of the elastic collisions for Ar used in the present paper from that in the previous one [4] is a result of the slightly different methodologies used to obtain $I(\varepsilon)$. In references [7, 8], the authors obtained the experimental data for α which is the cross-section in cm^2 of a cubic centimeter of gas at 0°C and a pressure of 1 mmHg. Reference [7] showed the relation between α and I to be $I = 10^{-20}\alpha/3.536$ m^2. Subsequently, I was calculated as indicated by the empty circles and triangles in Fig. 2. However, in the previous paper, we inferred the relation between α and I from Fig. 2 of reference [8]. Subsequently obtained I values are indicated by the "+" symbols in the bottom panel of Fig. 2. Therefore, the fitting results of $I(\varepsilon)$ in Fig. 2 in this paper match the experimental results more precisely than those in our previous paper.

In the collision model, we assume the anisotropic scattering in the center-of-mass frame. The anisotropic parameter, $d = 0.001$, is used to obtain the scattering angle of ions [4]. For $\varepsilon_i = 0.2$ eV and $n_n = 10^{19}$/m^3, the charge exchange collision frequency of He is equal to that of Ar with $\nu_{He} = \nu_{Ar} \sim 10^4$/s. Accordingly, the ratios of the gyrofrequencies to the collision frequencies are $\Omega_{He}/\nu_{He} = 100$ and $\Omega_{Ar}/\nu_{Ar} = 10$, indicating that the gyromotion of the He ions is less influenced by ion-neutral collisions than the Ar ions.

The test ion particles are initially located at $z < 0$ m within a small cylinder, shown in the gray region of Fig. 1. The volume of the small cylinder is $\pi a_{0,i}^2 v_{th,i}\Delta t_i$, where $a_{0,i}$ is the initial plasma radius, $v_{th,i}$ is the ion thermal velocity, and Δt_i is the simulation time step. Their initial velocities are given by a Maxwellian distribution with temperature T_i (in energy units), which defines the ion thermal velocity by $T_i = m_i v_{th,i}^2/2$. After $t = \Delta t_i$, some particles with a positive axial velocity of $v_z > 0$ cross $z = 0$ m and enter the region of $z > 0$ m. The ratio, β, of the number of ions that have crossed $z = 0$ m to the number of ions in the small cylinder is $\beta \sim 0.26$ for both ions. Then, the mass flow rate at $z = 0$ m is given by $\dot{m}_i = \beta m_i n_{0,i}\pi a_{0,i}^2 v_{th,i}$, where $n_{0,i}$ is the initial ion number density.

Several initial parameters are common to both propellant species, such as $T_i = 0.1$ eV and $n_{0,i} = n_n = 10^{19}$/m^3. The initial parameters that differ between the two species are summarized in Table 1, in which m_p is the proton mass, and $v_{b,i}$ is the average axial velocity of the particles that cross $z = 0$ m. The ratio of the thermal velocity of He to Ar is equal to the ratio of the average axial velocity of He to Ar, namely $v_{th,He}/v_{th,Ar} \sim v_{b,He}/v_{b,Ar} \sim (m_{Ar}/m_{He})^{1/2}$,

Table 1   Initial parameters for the He and Ar ions, where the ion temperature, $T_i = 0.1$ eV, and mass flow rate, $\dot{m} = 0.34$ mg/s, for both ion species.

	He	Ar
m_i	$4\,m_p$	$40\,m_p$
$v_{th,i}$	2.2 km/s	0.7 km/s
$v_{b,i} = \langle v_{z,i}\rangle$	1.8 km/s	0.57 km/s
$a_{0,i}$	5.3 cm	3 cm

because $T_{He} = T_{Ar}$ in the Maxwellian distributions with no drift. To compare the thrusts for the two ions with the same mass flow rate, the ratio of the initial plasma radii of He to Ar is determined as $a_{0,He}/a_{0,Ar} = (m_{Ar}/m_{He})^{1/4} \sim 1.78$ by using $\dot{m}_{He} = \dot{m}_{Ar}$. Here, $a_{0,Ar} = 0.03$ m is used, and $a_{0,He} = 0.053$ m is obtained. With these parameters, the mass flow rate is $\dot{m} = 0.34$ mg/s for both ions species. The thrust, F, is evaluated at $z = 2$ m by using the definition $F = \eta\dot{m}v_z$, where η is the ratio of the number of exhausted to injected particles and v_z is the average axial velocity of the exhausted particles.

3. Theory of Energy Gain

The perpendicular energy gain of ions due to the ICR is expressed by the quasilinear theory (QLT) as follows [4, 5];

$$\Delta\varepsilon_\perp = \frac{\pi}{4}\Phi_0\Lambda_B, \tag{1}$$

where $\Phi_0 = q_i^2 E_0^2/m_i\omega^2$ has a unit of energy, $\Lambda_B = L_B/\rho_z$ is the adiabatic parameter for the background magnetic field, and $\rho_z = v_{b,i}/\Omega_i(z_0)$ is a typical travel distance along z-axis during gyromotion. Here the QLT assumes an axially uniform electric field of $E_\perp(z) = E_0$ and a constant axial velocity of $v_{b,i}$.

The parallel energy gain of ions due to the PA can be described by the ponderomotive potential, $\Phi = q_i^2 E_\perp(z)^2/4m_i(\omega^2 - \Omega_i(z)^2)$, near gyroresonance. Here we assume $E_\perp(z) = E_0$ and $|z - z_0| = \rho_z$, leading to the gyrofrequency being approximately given by $\Omega_i(z) = \omega(1 - \rho_z/L_B)$. Assuming a large Λ_B in $\Phi(z)$, we obtain $\Delta\varepsilon_\parallel$ as follows:

$$\Delta\varepsilon_\parallel = \frac{1}{8}\Phi_0\Lambda_B. \tag{2}$$

Typically, $\Lambda_B = 100$ for Ar ions when $L_B = 1$ m and $\rho_z = 0.01$ m by using $v_{b,Ar} = 1$ km/s and $\Omega_{Ar} \sim 10^5$/s.

Equations (1) and (2) can qualitatively explain the numerical results for Ar ions, when $\Lambda_B < 100$ and $E_0 = 30$ V/m [4]. Therefore, the above theory based on the QLT and ponderomotive potential is useful to explain $\Delta\varepsilon$ in limited parameter regimes. In this paper, we also discuss the thrust in the same regimes. However, it is important to note that the theory fails to describe the energy gain for $\Lambda_B > 100$ [4]. The QLT neglects the effect of parallel acceleration, which reduces the transit time to cross

the acceleration region, leading to $\Delta\varepsilon$ becoming saturated for large Λ_B. The detailed investigation of the validity of our theory for the ICR/PA scheme is left for future work. Within the theory of Eqs. (1) and (2), the ratio of $\Delta\varepsilon_\parallel$ to $\Delta\varepsilon_\perp$ is constant with $\Delta\varepsilon_\parallel/\Delta\varepsilon_\perp = 1/2\pi$, representing an increase of approximately 16% in the energy gain for the ICR/PA compared with the energy gain in the ICR-only case.

In this paper, we compare the numerical results of the exhaust velocity dependence on ion mass with the theoretical predictions. The energy gain by the ICR/PA can be expressed by using Eqs. (1) and (2) as $\Delta\varepsilon_{ICR/PA} = \Delta\varepsilon_\perp + \Delta\varepsilon_\parallel \sim (2\pi + 1)\Phi_0\Lambda_B/8$. The exhaust velocity is then expressed as follows:

$$v_{z,i} = \sqrt{\frac{2\pi + 1}{4}\Lambda_B}\frac{E_0}{B_0}, \tag{3}$$

where the perpendicular energy gain due to the ICR is assumed to be completely converted into parallel energy. Then, the theoretically predicted ratio of the exhaust velocity of He to Ar is $v_{z,He}/v_{z,Ar} = (m_{Ar}/m_{He})^{1/4} \sim 1.78$.

4. Numerical Results

Figure 3 shows a snapshot of the motion of the He ions at $t = 1.5 \times 10^5 \Delta t_{He} \sim 1.5$ ms. At this time, the system had already reached a steady state. The parameter used is $E_0 = 40$ V/m. The top and bottom panels show the axial velocity (v_z) and perpendicular position (x), respectively, as functions of the axial position (z). At every time step, particles are introduced from the left-hand side boundary.
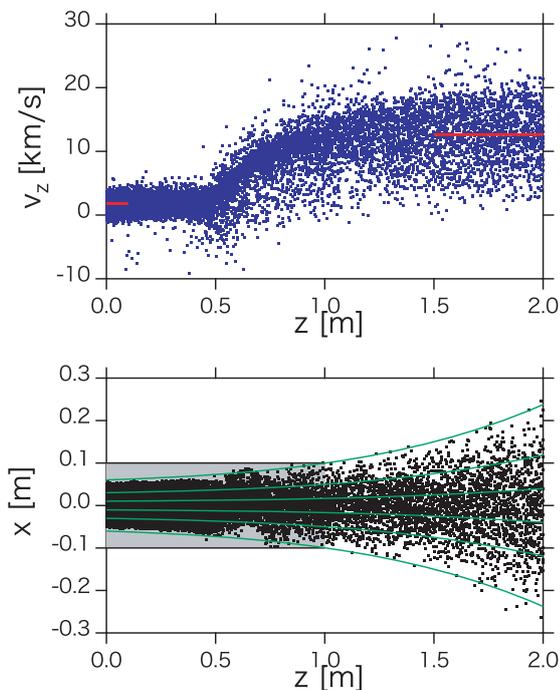
In the top panel, the injected and exhaust axial mean velocities are $v_{b,He} \sim 1.8$ km/s and $v_{z,He} \sim 12.6$ km/s (at 1.5 m $< z < 2$ m), respectively, shown by the solid red lines. In the bottom panel, the shaded region and solid green lines indicate the inside area of the chamber and background magnetic field lines, respectively. Most of the injected particles are exhausted from the chamber at $z = 1$ m without ion wall loss because the typical gyroradius is smaller than the device radius of 0.1 m.

Figure 4 is the same as Fig. 3, except that the ion species is Ar and the number of calculation time steps is 1.5×10^4, leading to the same calculation time as in Fig. 3. In the top panel, the injected and exhaust axial mean velocities are $v_{b,Ar} \sim 0.57$ km/s and $v_{z,Ar} \sim 3.0$ km/s (at 1.5 m $< z < 2$ m), respectively, shown by the solid red lines. The exhaust mean velocity for the He ions is larger than for the Ar ions with $v_{z,He} \sim 4v_{z,Ar}$. The larger exhaust velocity for the He ions is qualitatively explained by Eq. (3). However, the theory on which Eq. (3) is based predicts that $v_{z,He} \sim 31.8$ km/s and $v_{z,Ar} \sim 17.9$ km/s. These values are much larger than the numerically obtained values of v_z for both ion species. These discrepancies exist for the following two reasons: 1) shorter transit time near the resonance region due to parallel acceleration, as discussed in Section 3, and 2) the effect of ion-neutral collisions.

We estimate the thrust, $F = \eta\dot{m}_i v_z$, by using η and v_z at $z = 2$ m. Figures 5 and 6 show the numerically obtained values for v_z, η, and F as functions of E_0 for He and Ar, respectively. The results of different runs with and without ion wall loss and ion-neutral collisions are shown by

Fig. 3 Snapshot of the motion of the particles at $t = 1.5$ ms in (top) the $v_z - z$ and (bottom) $x - z$ spaces for the He ions.
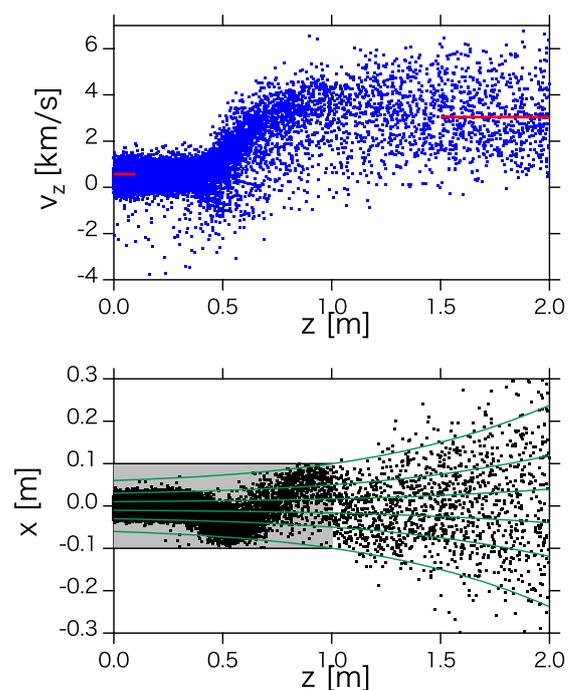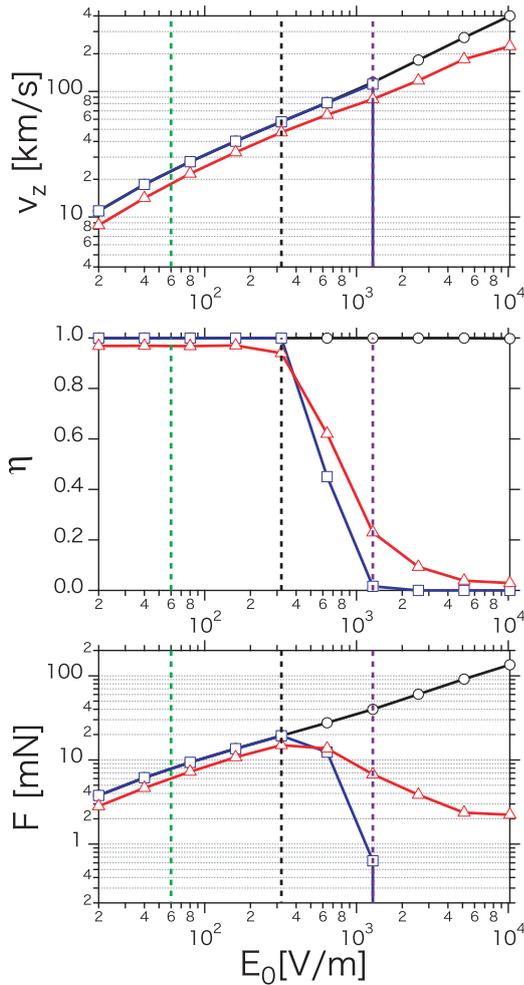

Fig. 4 Snapshot of the motion of the particles at $t = 1.5$ ms in (top) the $v_z - z$ and (bottom) $x - z$ spaces for the Ar ions.

Fig. 5 (Top) Exhaust velocity v_z, (middle) exhaust rate η, and (bottom) thrust F vs. electric field intensity for He. The symbols represent the numerical results without wall loss and collisions ($\circ$), with wall loss but without collisions ($\square$), and with wall loss and collisions ($\triangle$). The green, black, and purple dashed lines indicate $E_0 = 60\,\mathrm{V/m}$, $E_0 = 320\,\mathrm{V/m}$, and $E_0 = 1280\,\mathrm{V/m}$, respectively.
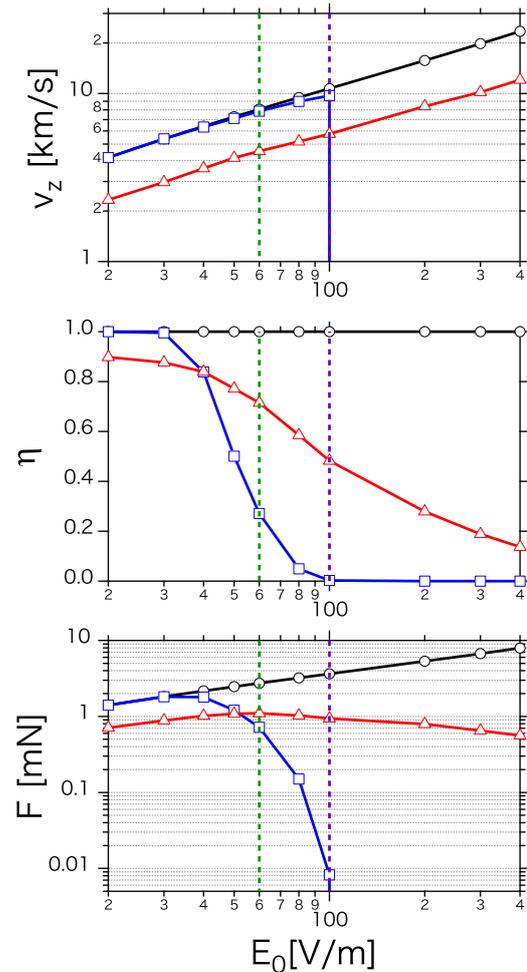
Fig. 6 (Top) Exhaust velocity v_z, (middle) exhaust rate η, and (bottom) thrust F vs. electric field intensity for Ar. The symbols represent the numerical results without wall loss and collisions ($\circ$), with wall loss but without collisions ($\square$), and with wall loss and collisions ($\triangle$). The green and purple dashed lines indicate $E_0 = 60\,\mathrm{V/m}$ and $E_0 = 100\,\mathrm{V/m}$, respectively.

different symbols. First, we examine v_z. For both ions, v_z increases with E_0. By comparing the runs between the runs with ion-neutral collisions (shown by the red triangles) and the runs without ion-neutral collisions (shown by the black circles), it is found that when $E_0 = 60\,\mathrm{V/m}$, the ion-neutral collision effects reduce v_z by 23% and 44% for He and Ar, respectively. These results show that the He ions are less influenced by ion-neutral collisions compared with the Ar ions because $\Omega_{\mathrm{He}}/\nu_{\mathrm{He}} > \Omega_{\mathrm{Ar}}/\nu_{\mathrm{Ar}}$, as discussed in Section 2.

Second, we examine η. As E_0 is increased, η decreases for the runs with ion wall loss (shown by the blue squares and red triangles) because the ion gyroradius increases with $\Delta\varepsilon_\perp$ due to the ICR, enhancing the effect of ion wall loss. The runs with ion wall loss and without ion-neutral collisions (shown by the blue squares) show that $\eta = 0$ at $E_0 \geq 1280\,\mathrm{V/m}$ and $E_0 \geq 100\,\mathrm{V/m}$ for the He

and Ar ions, respectively. At the critical E_0, the ion gyroradius for each ion is just equal to the chamber radius of 0.1 m, where $v_{z,\mathrm{He}} \sim 100\,\mathrm{km/s}$ and $v_{z,\mathrm{Ar}} \sim 10\,\mathrm{km/s}$, as shown by the blue squares in the top panel of each figure. Therefore, the strong ion wall loss beyond the critical E_0 is because of the increased gyroradius due to the ICR. At the same electric field intensity of $E_0 = 60\,\mathrm{V/m}$, η for the He ions is larger than for the Ar ions because the gyroradius of the He ions ($\sim 0.025\,\mathrm{m}$) is smaller than that of the Ar ions ($\sim 0.08\,\mathrm{m}$). Here we assume that the perpendicular velocity near the resonance is equal to v_z at $z = 2\,\mathrm{m}$ in a complete energy conversion from the perpendicular to parallel direction. Then, the gyroradius is determined by using v_z without either ion wall loss or ion-neutral collisions (shown by the black circles) in each top panel. Therefore, the He ions are less influenced by ion wall loss because of

Table 2   Output parameters at which thrust, along with both ion wall loss and ion-neutral collisions, is maximized for He and Ar.

	Helium	Argon
E_0	320 V/m	60 V/m
v_z	47 km/s	4.5 km/s
η	0.94	0.71
F	15 mN	1.1 mN
I_{sp}	4800 s	463 s

smaller gyroradius compared with the Ar ions.

Finally, we examine F. When the effects of both ion wall loss and ion-neutral collisions are included (shown by the red triangles), F is maximized, as a result of multiplying η and v_z. The output parameters at which F is maximumized are summarized in Table 2, where I_{sp} is the specific impulse defined by $I_{sp} = v_z/g$ and g is the gravitational acceleration constant. It is found that F_{He} and $I_{sp,He}$ are 13.6 times and 10 times larger than F_{Ar} and $I_{sp,Ar}$ under the same mass flow rate, respectively. Therefore, He is preferable to Ar as the propellant for the ICR/PA electric thruster. Here we compare F_{He} and F_{Ar} at the same electric field intensity of $E_0 = 60$ V/m. When the effects of both ion wall loss and ion-neutral collisions are not included (shown by the black circles), $F_{He}/F_{Ar} \sim 2.8$, where $F_{He} = 7.7$ mN and $F_{Ar} = 2.7$ mN. On the other hand, when the both effects are included (shown by the red triangles), $F_{He}/F_{Ar} \sim 5.4$, where $F_{He} = 6$ mN and $F_{Ar} = 1.1$ mN. Hence, we find that F_{He}/F_{Ar} increases because of the effects of ion wall loss and ion-neutral collisions, suggesting that He is less influenced than Ar by both those effects.

5. Summary and Discussion

We have studied the performance of an electrodeless electric thruster utilizing an ion cyclotron resonance/ponderomotive acceleration (ICR/PA) scheme, by utilizing the test particle simulations. We have compared the thrusts provided by using He and Ar gas as propellants at the same mass flow rate, along with the effects of both ion wall loss and ion-neutral collisions. The He ions are less influenced by both ion wall loss and ion-neutral collisions in comparison with the Ar ions because the gyroradius of the He ions is generally smaller than that of the Ar ions, and the ratio of the gyrofrequency to the collision frequency for the He ions is larger than that for the Ar ions. In addition, the exhaust velocity of the He ions is larger than that of the Ar ions. This is qualitatively explained by Eq. (3), which is based on the quasilinear theory (QLT) and ponderomotive potential. Accordingly, the thrust provided by He is larger than that of Ar under the same mass flow rate of $\dot{m} = 0.34$ mg/s. The thrust, F, for He reaches a maximum value of 15 mN at which the specific impulse,

I_{sp}, is 4800 s, whereas the maximum F attained for Ar is 1 mN with $I_{sp} = 463$ s. In conclusion, He is preferable as a propellant species for an electric thruster using the ICR/PA scheme compared with Ar. The parameters used are as follows. The maximum intensity and width of the rf electric field are 320 V/m and 0.1 m, respectively. The intensity at the resonance point and axial divergent scale length (L_B) of the background magnetic field are 0.04 T and 1 m, respectively. The radius and axial length of the cylindrical chamber are 0.1 m and 1 m, respectively. The initial velocities of ions obey a Maxwellian distribution with a temperature of $T_i = 0.1$ eV. The frequencies of the applied rf fields are 153 kHz and 15.4 kHz for the He and Ar ions, respectively.

Equations (1) and (2) based on the QLT and ponderomotive potential describes that the energy gain, $\Delta\varepsilon$, due to the ICR/PA is approximately proportional to the adiabatic parameter, $\Lambda_B = L_B/v_{b,i}\Omega_i$, where $v_{b,i}$ is the initial mean axial velocity for the injected particles and Ω_i is the ion gyrofrequency at resonance. In the present model with no drift of the ions, $v_{b,i}$ is of the same order of magnitude as the ion thermal velocity, $v_{th,i}$, so that the thrust created by the ICR/PA varies according to T_i. However, when an entire plasma drift initially exists, $v_{b,i}$ should be larger than $v_{th,i}$, so that the thrust will change according to the drift. A faster incoming plasma flow will reduce the thrust because a smaller Λ_B reduces $\Delta\varepsilon$. In future work, we need to investigate the thruster performance by considering the drift velocity of helicon plasma.

The theoretical estimate shows that the contribution of the PA to the energy gain is small compared with that of the ICR, namely $\Delta\varepsilon_\parallel/\Delta\varepsilon_\perp = 1/2\pi$. If we assume that only ICR is responsible for the axial exhaust velocity of the ions, then ion wall loss can be quantitatively explained. Therefore, the PA may not effectively contribute to the thrust with the parameters used here. However, we observed discrepancies between the exhaust velocities obtained by simulation and theory. A correct description of the energy gain by the ICR/PA beyond theory is left for future work. For making more realistic estimates, the perfect penetration of the externally applied rf field into magnetized plasmas should be modified from the present model. We have initiated a proof-of-principle experiment of this scheme using the Tokai Helicon Device (THD) [9–11], including the collision effect as well as the plasma-wall interaction.

[1] S. Shinohara, H. Nishida, K. Yokoi, T. Nakamura, T. Tanikawa, T. Hada, F. Otsuka, T. Motomura, E. Ohno, Funaki, T. Matsuoka, K.P. Shamrai and T.S. Rudenko, 32nd

Int. Electric Propul. Conf., IEPC-2011-056, Wiesbaden, 11-15 Sept. (2011).

[2] E.A. Bering III, F.R. Chang Díaz, J.P. Squire, T.W. Glover, M.D. Carter, G.E. McCaskill, B.W. Longmier, M.S. Brukardt, W.J. Chancery and V.T. Jacobson, Phys. Plasmas **17**, 043509 (2010).

[3] C. Charles, Plasma Sources Sci. Technol. **16**, R1 (2007).

[4] F. Otsuka, T. Hada, S. Shinohara, T. Tanikawa and T. Matsuoka, Plasma Fusion Res **8**, 1406012 (2013).

[5] I.Y. Dodin, N.J. Fisch and J.M. Rax, Phys. Plasmas **11**, 5046 (2004).

[6] V. Vahedi and M. Surendra, Comput. Phys. Commun. **87**, 179 (1995).

[7] W.H. Cramer and J.H. Simons, J. Chem. Phys. **26**, 1272 (1957).

[8] W.H. Cramer, J. Chem. Phys. **30**, 641 (1959).

[9] T. Tanikawa, S. Shinohara, Y. Ikeda, T. Hada and K. Toki, Bull. Am. Phys. Soc. **51**, 164 (2006).

[10] T. Tanikawa and S. Shinohara, Bull. Am. Phys. Soc. **53**, 175 (2008).

[11] T. Tanikawa, S. Shinohara and T. Motomura, Proceedings of Tokai U., RIST **31**, 4-11, in Japanese (2010).